Annals of Nuclear Energy 132 (2019) 227–235

Contents lists available at ScienceDirect

Annals of Nuclear Energy

journal homepage: www.elsevier.com/locate/anucene

Multiphysics analysis of the MSFR helium bubbling system: A comparison between neutron diffusion, SP_3 neutron transport and Monte Carlo approaches

Eric Cervi, Stefano Lorenzi, Lelio Luzzi *, Antonio Cammi

Politecnico di Milano, Energy Department, Via La Masa 34, 20156 Milan, Italy

ARTICLE INFO

Article history:
Received 16 January 2019
Received in revised form 16 April 2019
Accepted 18 April 2019

Keywords:
Molten Salt Reactor
Monte Carlo method
Multiphysics
Two-phase Euler-Euler solver

ABSTRACT

The Molten Salt Fast Reactor is a fast-spectrum molten salt reactor under development in the framework of the European H2020 SAMOFAR Project (http://samofar.eu/). Among the design peculiarities, this circulating fuel reactor features a helium bubbling system aimed at removing on-line gaseous fission products, and metallic particles as well. From a modelling point of view, the presence of helium bubbles in the core needs to be assessed both from a neutronics and thermal-hydraulics point of view. In this paper, the attention is paid to the first aspect, analysing the void reactivity effect induced by the bubbles by means of a Monte Carlo, an SP_3 neutron transport and a neutron diffusion approach. Since the distribution of helium bubbles is not uniform in the core but strongly depends on the fuel salt flow conditions, as well as on the location of their injection and extraction, a coupling scheme between Serpent 2 and OpenFOAM codes is adopted for the Monte Carlo analysis. In this way, the Monte Carlo code Serpent 2 is provided with a real bubble distribution calculated by means of a two-phase Euler-Euler solver implemented in OpenFOAM. The outcome puts in evidence the difference arising when a uniform and a real distribution of bubbles is considered in a Monte Carlo calculation. These results are also compared with an SP_3 neutron transport and a neutron diffusion solver implemented in OpenFOAM, highlighting the difference among the three neutronics approaches herein adopted.

1. Introduction

The Molten Salt Fast Reactor (MSFR) is a fast-spectrum molten salt reactor under development in the framework of the European H2020 SAMOFAR Project (http://samofar.eu/). In this circulating fuel reactor, the choice of a molten fluoride salt, acting both as fuel and coolant, leads to peculiar characteristics, such as the drift of the delayed neutron precursors, the strong coupling between neutronics and thermal-hydraulics, and the internal heat generation in the fluid (Serp et al., 2014). In addition, the current design of the MSFR foresees an on-line bubbling system for removing both the gaseous fission products via dilution and the metallic particles via capillary sticking (Delpech et al., 2009). A carrier gas (i.e., helium) is injected in the fuel circuit from the bottom, put in contact with the fuel salt, and extracted from the top. The schematic layout of the system is presented in Fig. 1, while its main design parameters are listed in Table 1.

The presence of helium bubbles in the core may affect both the neutronics and the thermal-hydraulic behaviour of the reactor. As for the latter, with limited flow rate, the presence of bubbles has a small impact on the temperature and velocity fields.

On the other hand, as far as neutronics is concerned, the void reactivity feedback of the bubbles is strongly dependent on the bubble spatial distribution. The contribution of the void reactivity effect is different if the bubbles are close to the centre of the core (where the neutron importance is higher) or are located in the periphery (where the neutron importance is lower). For this reason, a correct assessment of the void reactivity effect cannot be performed without the analysis of the bubble distribution, provided by a thermal-hydraulic simulation. In addition, the bubbles may have an important effect in some prompt-critical accident initiators, where the fuel compressibility cannot be neglected (Aufiero et al., 2017; Cervi et al., 2018a; Cervi et al., 2019). Again, the bubble spatial distribution is expected to have a relevant impact on the system dynamics, locally modifying the fuel compressibility. Therefore, a detailed analysis of the bubbly flow is important not only for steady-state criticality calculations, but also for transient simulation.

* Corresponding author.
E-mail address: lelio.luzzi@polimi.it (L. Luzzi).

https://doi.org/10.1016/j.anucene.2019.04.029
0306-4549/

Nomenclature

Latin symbols

c	Delayed neutron precursor density, m^{-3}
D	Neutron diffusion coefficient, m
d	Decay heat precursor density, W m^{-3}
$\boldsymbol{g}$	Gravitational acceleration, m s^{-2}
h	Specific enthalpy, J kg^{-1}
K	Modified thermal diffusivity, J m^{-1} s^{-1} K^{-1}
k_{eff}	Effective multiplication factor, –
L	Inter-phase heat transfer coefficient, W m^{-3}
M	Inter-phase momentum transfer, kg m^{-2} s^{-2}
p	Pressure, Pa
pcm	per cent mille (=10^{-5})
Q	Power source density, W m^{-3}
S	Mass source, kg m^{-3} s^{-1}
t	Time, s
$\boldsymbol{u}$	Velocity, m s^{-1}
v	Neutron velocity, m s^{-1}

Greek symbols

α	Gas fraction, –
$\bar{\alpha}_b$	Core average void fraction, –
α_i	Albedo coefficient, –
α_v	Void reactivity coefficient, pcm/%
β	Delayed neutron precursor fraction, –
β_{heat}	Decay heat energy fraction, –
ΔT	Inter-phase temperature difference, K
λ	Delayed neutron precursor decay constant, s^{-1}
λ_h	Decay heat precursor decay constant, s^{-1}
μ	Dynamic viscosity, Pa s
ν	Kinematic viscosity, m^2 s^{-1}
$\bar{\nu}$	Average neutrons per fission, –
ρ	Density, kg m^{-3}
$\tilde{\rho}$	Reactivity, pcm
$\sum$	Macroscopic cross section, m^{-2}
φ	Neutron flux, m^{-2} s^{-1} (diffusion equation)
φ_o	Neutron flux, m^{-2} s^{-1} (SP_3 equation)
φ_2	Neutron flux second moment, m^{-2} s^{-1}
χ	Neutron yield, –

Subscripts

b	Bubble
d	Delayed
f	Fission
h	Decay heat
i	Neutron energy group
j	Phase
k	Delayed neutron precursor group
m	Decay heat precursor group
p	Prompt
r	Removal
s	Scattering
$s2$	Second order scattering
$s3$	Third order scattering
T	Turbulent
t	Total
tr	Transport

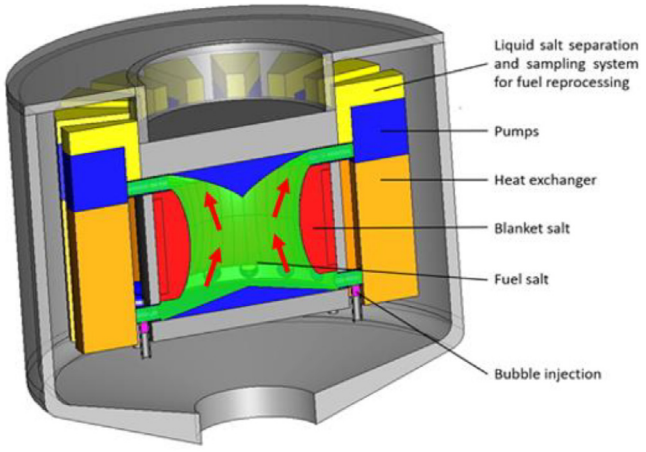

Fig. 1. Layout of the MSFR (the red arrows indicate the fuel flow direction).

Table 1
Main design parameters of the MSFR (Gerardin et al., 2017; Tano et al., 2017).

Parameter	Value
Nominal power	3000 MW_{th}
Fuel inlet temperature	923 K
Fuel outlet temperature	1023 K
Total salt volume	18 m^3
Salt composition (% mol.)	Fuel: LiF (77.5) – ThF_4 (20.0) – $^{233}UF_4$ (2.5) Fertile blanket: LiF (77.5) – ThF_4 (22.5)

The methodology adopted in this work and the obtained results are presented in Section 2, while conclusions are provided in Section 3.

2. Methodology and results

In this paper, the analysis of the void reactivity effect induced by the helium bubbling system in the MSFR is studied by comparing a neutron diffusion (Cervi et al., 2019) and an SP_3 neutron transport solver (Cervi et al., 2018b; Cervi et al., 2019b) with a Monte Carlo approach.

Neutron diffusion is typically selected for the estimation of the neutron flux in available multiphysics models of the MSFR (Fiorina et al., 2013; Aufiero et al., 2014a; Aufiero et al., 2014b; Fiorina et al., 2014). However, the adoption of more accurate neutronics models, based on transport theory, may constitute an improvement for the analysis of the MSFR, allowing for catching phenomena that cannot be described by means of diffusion approaches. It is well known that diffusion theory has some limits, especially when it comes to predicting the neutron behaviour in heterogeneous systems (Stacey, 2007). Hence, the neutronics analysis of the MSFR may benefit from the adoption of a neutron transport model, especially when non-homogeneous bubble distributions are involved. In this regard, the SP_3 approximation of the neutron transport equation (Brantley and Larsen, 2000) represents an improvement, compared to diffusion theory, in the analysis of the MSFR helium bubbling system. At the same time, this approach is characterized by lower computational requirements compared to more accurate neutronics models (e.g., S_N or integral

approaches), being therefore suitable for complex multiphysics simulations.

The deterministic (diffusion and SP_3) simulations are carried out with a multiphysics OpenFOAM solver developed for the analysis of the MSFR, coupling neutronics with a two-phase, compressible thermal-hydraulics model (Cervi et al., 2017; Cervi et al., 2018a). On the other hand, the Monte Carlo simulations are carried out using Serpent 2 (Leppänen et al., 2015), importing the bubble spatial distribution from the aforementioned OpenFOAM solver.

2.1. Deterministic approach

In the deterministic approach, a multiphysics solver developed in previous works (Cervi et al., 2017; Cervi et al., 2018a,b, 2019a,b) is used for assessing the reactivity due to the bubbling system (Fig. 2). The thermal-hydraulics sub-solver is based on the standard OpenFOAM solver *"twoPhaseEulerFoam"*, which adopts a Euler-Euler approach for compressible fluid and the bubble modelling. The neutronics sub-solver implements the multi-group SP_3 equation and, in alternative, the multi-group diffusion equation for the neutron flux and balance equations for the delayed neutron and decay heat precursor densities.

This model can be used in two different modes:

1. A time-independent, criticality mode, in which the system multiplication factor is evaluated at steady-state conditions. To this aim, a power iteration routine, based on the *k*-eigenvalue method (Bell and Glasstone, 1970) is implemented into the neutronics module (Cervi et al., 2017);
2. A time-dependent mode, for the analysis of operational as well as accidental transients.

At the beginning of each time (or power iteration) step, the thermal-hydraulics cycle solves for the phase fractions, for the velocity of both phases, for the pressure, and for the temperature. Picard iterations are performed until convergence is reached for the solution of the thermal hydraulic part of the problem. Then, the neutronics cycle begins, solving for the flux, for the delayed neutron precursors, and for the decay heat. Once the flux (the fission power in turn) and the decay heat are known, the volumetric power source field is updated, and the energy equation is solved again. Once the new temperature and density fields of the fuel are calculated, the cross sections are updated, also correcting for the void fraction (see Section 2.1.2, Eq. (9)), and the cycle is repeated with Picard iterations until convergence is reached. In addition, a certain number of external iterations – selectable by the user – between the thermal-hydraulics and the neutronics sub-solvers can be performed. The external iterations are particularly important in fast transients, in which the large thermal expansions due to steep power excursions have a strong impact on fuel velocity field.

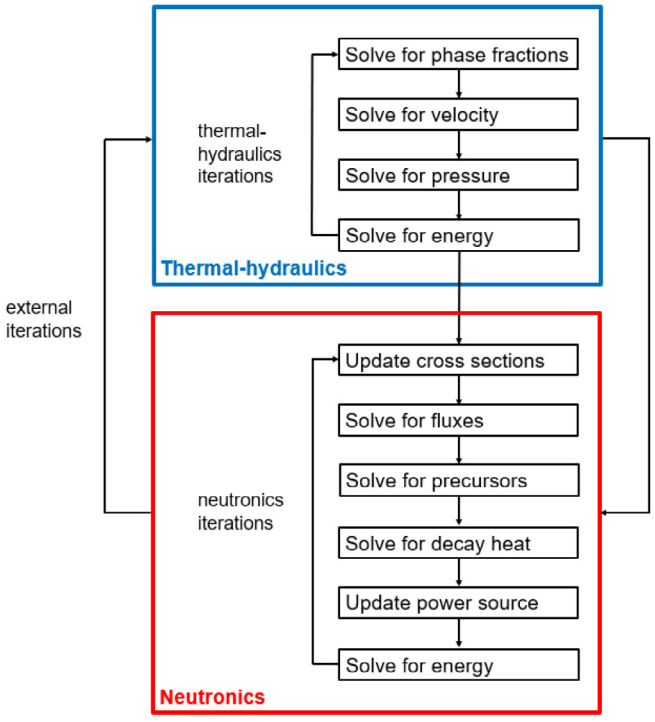

Fig. 2. Structure of the multiphysics solver.

Summarizing, the following information is exchanged between the two sub-solvers. The void fraction, fuel temperature and density are passed from thermal-hydraulics to neutronics, in order to evaluate the cross sections. On the other hand, the power density distribution is passed from the neutronics to the thermal-hydraulics solver, in order to update temperature. Then, once convergence is reached for both the neutronics and thermal-hydraulics solutions, the solver proceeds to the next time (or power iteration) step.

2.1.1. Thermal-hydraulics model

The need for a two-phase thermal-hydraulics solver is due to the presence of the online bubbling system foreseen for fission product removal and reactivity control. To this aim, the "*twoPhaseEulerFoam*" solver available in the OpenFOAM library is used, which implements an Euler-Euler approach (Rusche, 2002). Each phase is treated as a continuum interpenetrating each other, and is described with averaged conservation equations. Due to the averaging process, phase fractions are introduced into the governing equations.

The mass and momentum conservation equations for the two phases read:

$$\begin{cases} \frac{\partial(\rho_j\alpha_j)}{\partial t} + \nabla\cdot\left(\rho_j\alpha_j\boldsymbol{u}_j\right) = S_j \\ \frac{\partial\rho_j\alpha_j\boldsymbol{u}_j}{\partial t} + \nabla\cdot\left(\rho_j\alpha_j\boldsymbol{u}_j\boldsymbol{u}_j\right) \\ = \nabla\cdot\alpha_j\left[-p\boldsymbol{I} + (\mu+\mu_t)\left(\nabla\boldsymbol{u} + (\nabla\boldsymbol{u})^T\right) - \frac{2}{3}\mu(\nabla\cdot\boldsymbol{u})\boldsymbol{I}\right] + M_j \end{cases} \quad (1)$$

A mass source term S_j is considered in the continuity equation to model gas injection and extraction in the reactor. The term M_j appears in the averaged momentum equations of each phase due to non-linearity, which requires closure equations. This term takes into account the momentum transfer between the two phases, due to the forces acting at the liquid-gas interface, namely the lift, the drag, virtual mass forces and turbulent dispersions. Several models are implemented into the solver to describe the inter-phase terms and to close the momentum equation (Gidaspow, 1994; Enwald et al., 1996).

The energy equations for the two-phases for the "*twoPhaseEulerFoam*" read:

$$\begin{aligned} &\frac{\partial\rho_j\alpha_j h_j}{\partial t} + \nabla\cdot\left(\rho_j\alpha_j\boldsymbol{u}_j h_j\right) + \frac{\partial\rho_j\alpha_j k_j}{\partial t} + \nabla\cdot\left(\rho_j\alpha_j\boldsymbol{u}_j k_j\right) \\ &== \alpha_j\frac{\partial p}{\partial t} + \frac{\alpha_j}{\rho_j C_{p,j}}\nabla\cdot\left((K+K_t)\nabla h_j\right) + L\Delta T + \rho_j\alpha_j\boldsymbol{g}\cdot\boldsymbol{u}_j + Q_f + Q_h \end{aligned} \quad (2)$$

where L is an inter-phase heat transfer coefficient resulting from the averaging process and ΔT is the temperature difference between the two phases. Also in this case, different models are implemented in the solver and can be chosen to describe L, closing the energy equation (Ranz and Marshall, 1952).

2.1.2. SP_3 neutronics model

The SP_3 multi-group equation is selected for the estimation of the neutron flux:

$$\frac{1}{v_i}\frac{\partial \Phi_{0,i}}{\partial t} = \nabla \cdot D_{0,i}\nabla\Phi_{0,i} - \Sigma_{r,i}\left(\Phi_{0,i} - 2\varphi_{2,i}\right) + S_{n,i}(1-\beta)\chi_{p,i} + S_d\chi_{d,i} + S_{s,i} + \frac{2}{v_i}\frac{\partial \varphi_{2,i}}{\partial t} \quad (3)$$

$$\frac{9}{5}\frac{1}{v_i}\frac{\partial \varphi_{2,i}}{\partial t} = \nabla \cdot D_{2,i}\nabla\varphi_{2,i} - \Sigma_{t2,i}\varphi_{2,i} + \frac{2}{5}\Sigma_{r,i}\left(\Phi_{0,i} - 2\varphi_{2,i}\right) - \frac{2}{5}S_{n,i}(1-\beta)\chi_{p,i} - \frac{2}{5}S_d\chi_{d,i} - \frac{2}{5}S_{s,i} + \frac{2}{5}\frac{1}{v_i}\frac{\partial \Phi_{0,i}}{\partial t} \quad (4)$$

where $\Phi_{0,i}$ is defined as:

$$\Phi_{0,i} = \varphi_{0,i} + 2\varphi_{2,i} \quad (5)$$

In addition:

$$D_{0,i} = \frac{1}{\Sigma_{tr,i}} \quad (6)$$

$$\Sigma_{t2,i} = \Sigma_{t,i} - \Sigma_{s2,ii} \quad (7)$$

$$D_{2,i} = \frac{9}{35}\frac{1}{\Sigma_{t,i} - \Sigma_{s3,ii}} \quad (8)$$

The macroscopic cross sections are evaluated by assuming a logarithmic dependence on temperature and a linear dependence on density and on the void fraction due to the helium bubbles, according to the following relation:

$$\Sigma_{i,j} = \left[\Sigma^o_{i,j} + A_{i,j} log\frac{T_{fuel}}{T_{ref}}\right]\frac{\rho_{fuel}}{\rho_{ref,fuel}}(1-\alpha_b) \quad (9)$$

The source terms represent the fission neutrons, the scattering neutrons and the delayed neutrons, respectively, and are evaluated as follows:

$$S_{n,i} = \sum_j \bar{\nu}\,\Sigma_{f,j}\varphi_{0,j} \quad (10)$$

$$S_{s,i} = \sum_{j\neq i}\Sigma_{s,j\to i}\varphi_{0,j} \quad (11)$$

$$S_d = \sum_k \lambda_k c_k \quad (12)$$

Due to these explicit terms, an iterative procedure among the several groups is required to achieve convergence for the neutronics description. Albedo boundary conditions are adopted at the top and bottom walls of the reactor (axial reflectors) and at the radial wall (blanket salt), in order to limit the domain of the equation set of neutronics to the fuel salt circuit only (Aufiero et al., 2014b; Fiorina et al., 2017). For the SP_3 equations, the albedo boundary conditions can be applied, starting from the outgoing and the ingoing neutron currents, as follows:

$$D_{0,i}\nabla\Phi_{0,i} = -\frac{1}{2}\left(\frac{1-\alpha_i}{1+\alpha_i}\right)\left(\Phi_{0,i} - \frac{3}{4}\varphi_{2,i}\right) \quad (13)$$

$$D_{2,i}\nabla\varphi_{2,i} = \frac{1}{2}\left(\frac{1-\alpha_i}{1+\alpha_i}\right)\left(\frac{3}{20}\Phi_{0,i} - \frac{21}{20}\varphi_{2,i}\right) \quad (14)$$

where the albedo coefficients α_i are the ratios between the outgoing and the ingoing neutron currents.

The precursor balance equations include the diffusion and the transport term to allow for the fuel motion (neglecting the precursor mass transfer from the liquid to the gas phase):

$$\frac{\partial \rho_{\boldsymbol{l}}\alpha_{\boldsymbol{l}}c_k}{\partial t} + \nabla\cdot(\rho_{\boldsymbol{l}}\alpha_{\boldsymbol{l}}\boldsymbol{u}_{\boldsymbol{l}}c_k) = \nabla\cdot\left(\rho_{\boldsymbol{l}}\alpha_{\boldsymbol{l}}\left(\frac{\nu}{Sc} + \frac{\nu_T}{Sc_T}\right)\nabla c_k\right) + \beta_k\sum_i \bar{\nu}\,\Sigma_{f,i}\varphi_i - \lambda_k\rho_{\boldsymbol{l}}\alpha_{\boldsymbol{l}}c_k \quad (15)$$

The turbulent Schmidt number Sc_T is set to 0.85, even if no data are specifically available for the diffusion of species in the MSFR salt (Aufiero et al., 2014b).

In order to properly consider the decay heat during accidental transients, the solver is provided with equations that consider the behaviour of the isotopes responsible for the decay heat, subdivided in "decay heat groups" in a manner similar to the precursor groups. Actually, the equations implement the balance for the precursor concentration multiplied by the average energy released by that decay group:

$$\frac{\partial \rho_{\boldsymbol{l}}\alpha_{\boldsymbol{l}}d_m}{\partial t} + \nabla\cdot(\rho_{\boldsymbol{l}}\alpha_{\boldsymbol{l}}\boldsymbol{u}_{\boldsymbol{l}}d_m) = \nabla\cdot\left(\rho_{\boldsymbol{l}}\alpha_{\boldsymbol{l}}\left(\frac{\nu}{Sc} + \frac{\nu_t}{Sc_t}\right)\nabla d_m\right) + \beta_{h,l}\sum_i E_f\Sigma_{f,i}\varphi_i - \lambda_{h,l}\rho_{\boldsymbol{l}}\alpha_{\boldsymbol{l}}d_m \quad (16)$$

In addition, a power iteration routine, based on the k-eigenvalue method, is implemented in the neutronics module of the solver for the calculation of the multiplication factor. For a more detailed description, the reader is referred to (Cervi et al., 2017).

2.1.3. Diffusion neutronics model

In addition to the SP_3 module, a multi-group neutron diffusion solver is available for the evaluation of the flux. For the i-th energy group, the diffusion equation reads as follows:

$$\frac{1}{v_i}\frac{\partial \varphi_i}{\partial t} = \nabla\cdot D_i\nabla\varphi_i - \Sigma_{r,i}\varphi_i + S_{n,i}(1-\beta)\chi_{p,i} + S_d\chi_{d,i} + S_{s,i} \quad (17)$$

in which Eqs. (9) to (12) are used to describe the source terms and the cross section dependence on the fuel temperature and density and on the void fraction. For the diffusion equation, albedo boundary conditions are specified as follows:

$$D_i\nabla\varphi_i = -\frac{1}{2}\left(\frac{1-\alpha_i}{1+\alpha_i}\right)\varphi_i \quad (18)$$

The balance equations for the delayed neutron and decay heat precursors, Eqs. (15) and (16), are also implemented into the diffusion solver.

2.1.4. Analysis of the MSFR helium bubbling system

In this section, the coupled neutronics and thermal-hydraulics deterministic model is used to investigate the MSFR helium bubbling system, highlighting its impact on the system reactivity. The presence of the bubbly flow causes a negative reactivity insertion into the system due to the negative void coefficient. A preliminary evaluation of this contribution can be made considering a uniform void fraction (Brovchenko et al., 2013). On the other hand, the real distribution of the bubbly flow inside the reactor is not uniform since the bubble are transported by the fluid flow, i.e., the void reactivity feedback coefficient

$$\alpha_\nu = \frac{\Delta\tilde{\rho}}{\bar{\alpha}_b} \quad (19)$$

needs to be calculated accounting for the spatial and importance dependence of the bubble void feedback. The developed solver, thanks to the coupling between the neutronics and the two-phase thermal-hydraulic physics, is suitable to study the mentioned aspect of the void reactivity feedback.

The present analysis is carried out on a quarter of the MSFR full core (Figs. 3 and 4). In this work, 650 °C and 750 °C are taken as inlet and outlet temperature of the fuel salt, respectively, and a

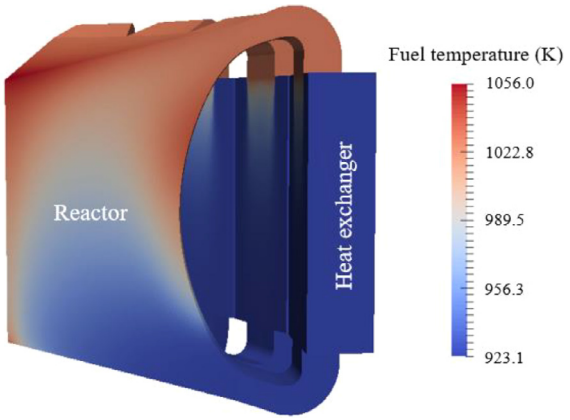

Fig. 3. Fuel temperature distribution.

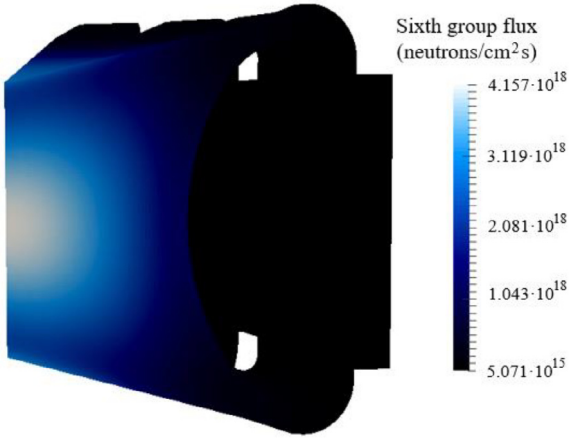

Fig. 4. Sixth group flux distribution.

full-core thermal power of 3000 MWth is assumed to normalize the neutron flux. Different helium flow rates are injected at the bottom of the reactor and all the gas is removed in the external circuit (Fig. 5a). The design specifications of the gas injection and extraction systems are still to be defined and their optimization is out of the scope of the present work. Therefore, helium injection and extraction are simply modelled by means of mass source/sink terms in the continuity equation. Similarly, the primary pumps are simulated by means of momentum sources, uniformly distributed in the heat exchanger regions. Albedo boundary conditions are adopted at the reactor walls, while symmetry is imposed at the cutting planes.

The multiplication factor is estimated at different core average void fractions with the power iteration routine implemented into the solver (Cervi et al., 2017), assuming both a uniform bubble distribution as well as the bubble distribution calculated by the multiphysics solver. Six-group constants are generated with Serpent 2, selecting the JEFF-3.1.1 library (Santamarina et al., 2009) for cross section data and using 100 million neutron histories (10^5 neutrons for 1000 cycles), obtaining a 5 pcm uncertainty on the multiplication factor. The energy group subdivision adopted in this work for the diffusion and SP_3 calculations is shown in Table 2. This energy structure has been tested in previous works (Fiorina, 2013; Fiorina et al., 2013) against ERANOS (using 33 and 1968 energy groups) and Serpent, showing that it is capable to reproduce the overall shape of the neutron spectrum. The Serpent model of the MSFR used for cross section generation is presented in Section 2.2.

The values of the multiplication factor and of the void reactivity feedback coefficient obtained with the SP_3 and the diffusion approaches are listed in Tables 3 and 4, respectively. The core average void fractions listed in the first column are evaluated at steady state for different bubble injection rates, i.e., 0, 3.6, 7.2 and 10.8 g/s, respectively.

Figs. 3 and 4 represent the temperature and the sixth group flux distributions in the three-dimensional geometry, obtained using the SP_3 solver for neutronics. In addition, Figs. 5 and 6 show the bubble and the power density distributions at 1.308% core-average void fraction. It can be observed that, in correspondence of the bubbly flow paths, the power density decreases, due the void feedback on the fission rate.

Table 2
Energy group division adopted in the present work.

Energy group	Energy ranges (MeV)
1	$2.23 \div 20.00$
2	$4.98 \cdot 10^{-1} \div 2.23$
3	$2.48 \cdot 10^{-2} \div 4.98 \cdot 10^{-1}$
4	$5.53 \cdot 10^{-3} \div 2.48 \cdot 10^{-2}$
5	$7.49 \cdot 10^{-4} \div 5.53 \cdot 10^{-3}$
6	$0 \div 7.49 \cdot 10^{-4}$

2.1.5. Discussion of results

As shown by Tables 3 and 4, if the void reactivity feedback coefficient is evaluated on the basis of the real bubble spatial distribution (Fig. 5), calculated with the coupled solver, the values of the multiplication factor and of the void reactivity feedback coefficient show significant differences compared to the simulations carried out with uniform void fractions. These outcomes highlight a strong dependence of the void feedback on the bubble spatial distribution as well as on the neutron importance. In particular, the void reactivity coefficient is higher compared to the uniform void fraction case, due to the larger bubble concentration in the central region of the core, where the neutron importance is higher. In this regard, the positions of the bubble injection and extraction systems have an important impact on the void reactivity coefficient, directly influencing the bubbly flow path.

2.2. Monte Carlo approach

The void coefficient due to the bubbles is usually calculated through Monte Carlo approach considering a uniform bubble dis-

Table 3
SP_3 approach: multiplication factor and void reactivity coefficient with uniform and calculated bubble distribution.

Core average void fraction (%)	Multiplication factor		α_v (pcm/%)	
	Uniform bubble distribution	Real bubble distribution	Uniform bubble distribution	Real bubble distribution
0	0.96581	0.96581	–	–
0.437	0.96511	0.96444	−171.8	−336.6
0.876	0.96434	0.96308	−180.2	−335.0
1.308	0.96360	0.96179	−181.5	−330.9

Table 4
Diffusion approach: multiplication factor and void reactivity coefficient with uniform and calculated bubble distribution.

Core average void fraction (%)	Multiplication factor		α_v(pcm/%)	
	Uniform bubble distribution	Real bubble distribution	Uniform bubble distribution	Real bubble distribution
0	0.96503	0.96503	–	–
0.437	0.96429	0.96364	−182.0	−342.0
0.876	0.96354	0.96227	−182.9	−339.3
1.308	0.96279	0.96097	−184.3	−334.7

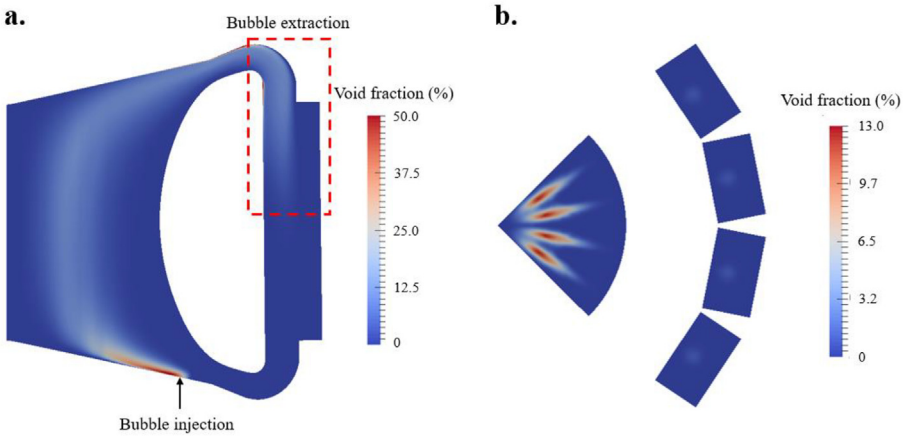

Fig. 5. Void fraction distribution at 1.308% core average void fraction. Vertical (a) and horizontal (b) sections.

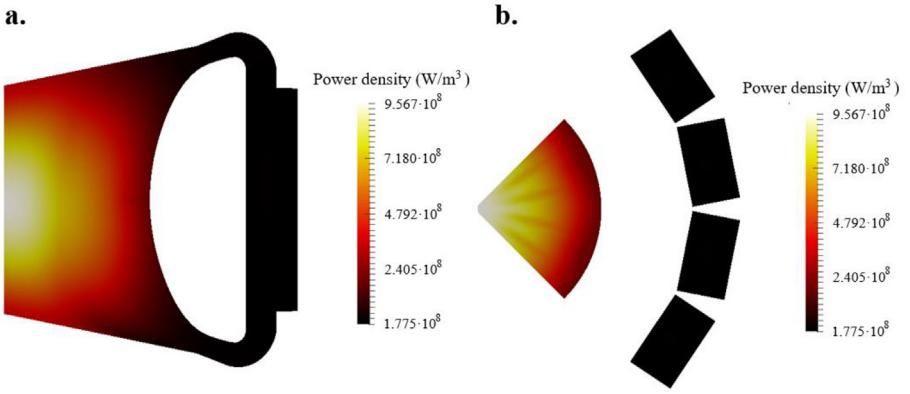

Fig. 6. Power density distribution at 1.308% core average void fraction, obtained with the SP_3 approach. Vertical (a) and horizontal (b) sections.

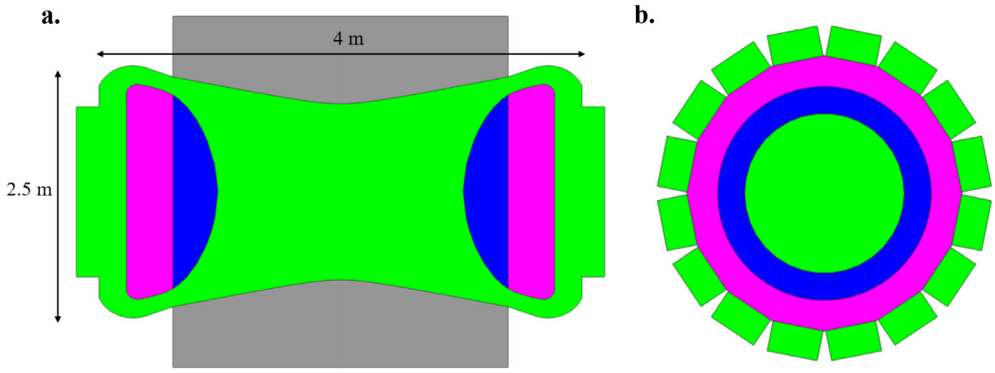

Fig. 7. Vertical (a) and horizontal (b) sections of the Serpent model. In green, the liquid fuel (reactor and external circuits), in blue the fertile blanket, in grey the reflectors and in purple the boron carbide shield. (For interpretation of the references to colour in this figure legend, the reader is referred to the web version of this article.)

Table 5
Monte Carlo approach: multiplication factor and void reactivity coefficient (±1-sigma uncertainty) with uniform and calculated bubble distribution.

Core average void fraction (%)	Multiplication factor		α_v (pcm/%)	
	Uniform bubble distribution	Real bubble distribution	Uniform bubble distribution	Real bubble distribution
0	0.97110 ± 0.00005	0.97110 ± 0.00005	–	–
0.437	0.97042 ± 0.00005	0.96980 ± 0.00005	−165.1 ± 17.2	−315.9 ± 17.2
0.876	0.96970 ± 0.00005	0.96855 ± 0.00005	−169.7 ± 8.6	−309.5 ± 8.6
1.308	0.96904 ± 0.00005	0.96731 ± 0.00005	−167.4 ± 5.8	−308.5 ± 5.8

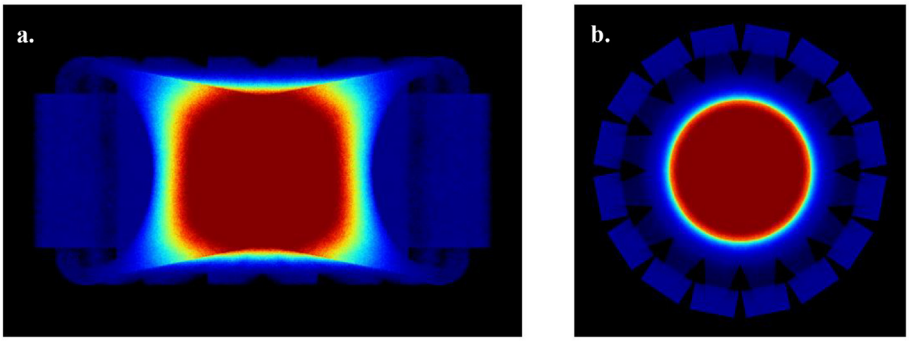

Fig. 8. Normalized fission rate distribution in arbitrary units (black = 0, red = 1) at 1.308% core average void fraction (real bubble distribution). Vertical (a) and horizontal (b) sections. (For interpretation of the references to colour in this figure legend, the reader is referred to the web version of this article.)

tribution, i.e., calculating a density-based effect (Brovchenko et al., 2013). On the other hand, as shown in the previous section, the spatial distribution of the bubbles can be very different from the uniform case. To this aim, for assessing the void reactivity coefficient in the MSFR, the bubble spatial distribution calculated with the two-phase Euler-Euler solver is exported into a Serpent model of the MSFR (Fig. 7) through a built-in multiphysics interface with OpenFOAM (Tuominen et al., 2016). Unlike the deterministic model, in which albedo boundary conditions are used at the reactor walls, the radial fertile blanket and the top and bottom reflectors are considered here. The present calculations are carried out using 100 million neutron histories, obtaining a 5 pcm uncertainty on the multiplication factor.

As in the previous section, simulations are carried out (i) assuming a uniform bubble distribution and (ii) importing the non-homogeneous bubble distribution calculated by the OpenFOAM solver. The values of the multiplication factor and of the void reactivity feedback coefficient obtained with the Monte Carlo approach are listed in Table 5. In addition, Fig. 8 shows the normalized fission rate distribution in the MSFR evaluated by Serpent.

Table 6
Multiplication factor difference between the SP_3 and the Monte Carlo approaches.

Core average void fraction (%)	$k_{eff.SP3} - k_{eff.MC}$ (pcm)	
	Uniform bubble distribution	Real bubble distribution
0	−529	−529
0.437	−531	−536
0.876	−536	−547
1.308	−544	−552

Table 7
Multiplication factor difference between the diffusion and the Monte Carlo approaches.

Core average void fraction (%)	$k_{eff.diff} - k_{eff.MC}$(pcm)	
	Uniform bubble distribution	Real bubble distribution
0	−607	−607
0.437	−613	−616
0.876	−616	−628
1.308	−625	−634

2.2.1. Discussion of results

The Monte Carlo results confirm that the void reactivity feedback is strongly dependent on the bubble spatial distribution, due to the aforementioned neutron importance effects. This consideration is not dependent on the choice of the neutronics model, since the same behaviour is observed using two deterministic approaches as well as a Monte Carlo one. Therefore, this is a physical effect that can only be described by means of an accurate thermal-hydraulics solver, which is able to handle the presence of bubbles inside the reactor and to reproduce their spatial distribution.

In general, good agreement is shown between the SP_3, the diffusion and the Monte Carlo results. The multiplication factor difference between the three approaches is shown in Tables 6 and 7.

The agreement between the three approaches is fairly good, also considering the large scale of the system and the complex multiphysics coupling between neutronics and two-phase thermal-hydraulics. In general, compared to Monte Carlo, the SP_3 and the diffusion solvers underestimate the multiplication factor. This result can be explained by considering that in the deterministic model: (i) the domain is limited to the fuel circuit without considering reflectors and fertile blanket zones (which are accounted for by means of albedo boundary conditions), and (ii) the precursor motion through the reactor is considered leading to a reduction of reactivity. In particular, in the deterministic model, part of the precursors decay outside the active zone without contributing to fissions.

Good agreement is also obtained in the prediction of the void reactivity coefficient, as shown by Tables 8 and 9. Beside the differences between the deterministic and the Monte Carlo approaches, a possible source of error may be represented by the albedo boundary conditions adopted in the deterministic model. In fact, the treatment of neutron leakages may have a relevant impact on the evaluation of the void reactivity feedback.

Table 8
Void coefficient relative difference between the SP_3 and the Monte Carlo approaches.

Core average void fraction (%)	α_v relative difference (%)	
	Uniform bubble distribution	Real bubble distribution
0	–	–
0.437	4.07	6.55
0.876	6.16	8.26
1.308	8.48	7.26

Table 9
Void coefficient relative difference between the diffusion and the Monte Carlo approaches.

Core average void fraction (%)	α_v relative difference (%)	
	Uniform bubble distribution	Real bubble distribution
0	–	–
0.437	10.24	8.26
0.876	7.78	9.63
1.308	10.10	8.49

As expected, the SP_3 solver is in better agreement with the Monte Carlo results, compared to the diffusion approach. Visible improvement is observed in the prediction of the multiplication factor, and of the void coefficient as well. Considering that the bottleneck in runtime is due to thermal-hydraulics, and not to neutronics, the use of the SP_3 solver only leads to an increase of about 17% of computational times, compared to the diffusion solver. In this regard, the adoption of an SP_3 approach represents a valuable addition to the multiphysics analysis of the MSFR, since (i) it is more accurate than neutron diffusion, without significantly increasing computational requirements, and (ii) it can be coupled with the moving precursor balance equations, as opposed to Monte Carlo methods which consider static fuel.

3. Conclusions

In this paper, the MSFR helium bubbling system and its effects on reactivity are investigated by means of an SP_3 neutron transport, a neutron diffusion and a Monte Carlo approach. The SP_3 and the diffusion models are implemented in a multiphysics OpenFOAM solver, including a two-phase thermal-hydraulics model to handle the presence of bubbles inside the reactor. On the other hand, Monte Carlo calculations are carried out with Serpent 2, which is particularly suitable for multiphysics simulations thanks to its interface with OpenFOAM. The void reactivity feedback coefficient is calculated: (i) using a uniform void fraction and (ii) on the basis of the real bubble distribution in the core (i.e., the bubble distribution calculated by the two-phase solver).

Significant differences arise between the outcomes of the two cases, pointing out that spatial as well as importance effects have a strong impact on the void reactivity feedback of the bubbles. These results highlight that an accurate calculation of the bubble spatial distribution is required to evaluate the void reactivity feedback coefficient of the reactor and, as a consequence, to develop coherent control strategies.

The outcomes of this work constitute the starting point for further research on the MSFR dynamics and transient analysis, with a particular focus on the analysis and the development of the reactivity control systems as well as of the optimization of the most relevant design features of the reactor (notably, the fuel composition, the operating temperatures, and the fuel flow rate). In particular, this study can be useful for the design of the bubble injection and extraction systems, providing guidelines for the optimization of their position in the reactor.

Finally, the present analysis is also aimed at highlighting the difference between a deterministic description of neutronics and a Monte Carlo approach. On one side, the six-group approximation and the albedo boundary conditions adopted in the SP_3 and in the diffusion models may be a source of error, compared to the Monte Carlo approach. On the other hand, standard Monte Carlo codes do not have the capability to model the precursor motion through the circulating fuel (except from a preliminary development presented by Aufiero et al., 2017), which is also fundamental for a correct estimation of reactivity in liquid fuel nuclear reactors. However, a general good agreement is obtained between the two approaches, both in the prediction of the multiplication factor and of the void reactivity coefficient.

Acknowledgments

This project has received funding from the EURATOM research and training programme 2014-2018 under grant agreement No 661891.

Disclaimer

The content of this paper does not reflect the official opinion of the European Union. Responsibility for the information and/or views expressed therein lies entirely with the authors.

References

Aufiero, M., Brovchenko, M., Cammi, A., Clifford, I., Geoffroy, O., Heuer, D., Laureau, A., Losa, M., Luzzi, L., Merle, E., Ricotti, M.E., 2014a. Calculating the effective delayed neutron fraction in the Molten Salt Fast Reactor: analytical, deterministic and Monte Carlo approaches. Ann. Nucl. Energy 65, 390–401.

Aufiero, M., Cammi, A., Geoffroy, O., Losa, M., Luzzi, L., Ricotti, M.E., Rouch, H., 2014b. Development of an OpenFOAM model for the Molten Salt Fast Reactor transient analysis. Chem. Eng. Sci. 111, 78–90.

Aufiero, M., Rubiolo, P., Fratoni, M., 2017. Monte Carlo/CFD coupling for accurate modelling of the delayed neutron precursors and compressibility effects in Molten Salt Reactors. Transactions of the American Nuclear Society. June 11-15.

Bell, G.I., Glasstone, S., 1970. Nuclear Reactor Theory. Van Nostrand Reinhold Company, New York.

Brantley, P.S., Larsen, E.W., 2000. The simplified P_3 Approximation. Nucl. Sci. Eng. 134, 1–21.

Brovchenko, M., Merle, E., Rouch, H., Alcaro, F., Allibert, M., Aufiero, M., Cammi, A., Dulla, S., Feynberg, O., Frima, L., Geoffroy, O., Heuer, D., Ignatiev, V., Kloosterman, J.L., Lathouwers, D., Laureau, A., Luzzi, L., Merk, B., Ravetto, P., Rineiski, A., Rubiolo, P., Rui, L., Szieverth, M., Wang, S., Yamaji, B., 2013. Optimization of the preconceptual design of the MSFR, EVOL D2-2 Report (Evaluation and Viability of Liquid Fuel Fast Reactor System).

Cervi, E., Lorenzi, S., Cammi, A., Luzzi, L., 2017. An Euler-Euler multi-physics solver for the analysis of the helium bubbling system in the MSFR. NENE 2017 26th International Conference Nuclear Energy for New Europe. September 11-14.

Cervi, E., Lorenzi, S., Cammi, A., Luzzi, L., 2018a. Analysis of the effect of fuel compressibility on super-prompt-critical dynamics of the Molten Salt Fast Reactor. PHYSOR 2018: Reactor Physics Paving The Way Towards More Efficient Systems. April 22-26.

Cervi, E., Lorenzi, S., Luzzi, L., Cammi, A., 2018b. An OpenFOAM solver for criticality safety assessment in dynamic compression events. Transactions of the American Nuclear Society. November 11-15.

Cervi, E., Lorenzi, S., Cammi, A., Luzzi, L., 2019a. Development of a multiphysics model for the study of fuel compressibility effects in the Molten Salt Fast Reactor. Chem. Eng. Sci. 193, 379–393.

Cervi, E., Lorenzi, S., Cammi, A., Luzzi, L., 2019b. Development of an SP_3 neutron transport solver for the analysis of the Molten Salt Fast Reactor. Nucl. Eng. Design 346, 209–219.

Delpech, S., Merle, E., Heuer, D., Allibert, A., Ghetta, V., Le-Brun, C., Mathieu, L., Picard, G., 2009. Reactor physics and reprocessing scheme for innovative molten salt reactor system. J. Fluor. Chem. 130, 11–17.

Enwald, H., Peirano, E., Almstedt, A.E., 1996. Eulerian two-phase flow theory applied to fluidization. Int. J. Multiphase Flow 22, 21–66.

Fiorina, C., 2013. The molten salt fast reactor as a fast spectrum candidate for thorium implementation, PhD thesis.

Fiorina, C., Aufiero, M., Cammi, A., Franceschini, F., Krepel, J., Luzzi, L., Mikityuk, K., Ricotti, M.E., 2013. Investigation of the MSFR core physics and fuel cycle characteristics. Progr. Nucl. Energy 68, 153–158.

Fiorina, C., Lathouwers, D., Aufiero, M., Cammi, A., Guerrieri, C., Kloosterman, J.L., Luzzi, L., Ricotti, M.E., 2014. Modelling and analysis of the MSFR transient behaviour. Ann. Nucl. Energy 64, 485–498.
Fiorina, C., Hursin, M., Pautz, A., 2017. Extension of the GeN-foam neutronic solver to SP_3 analysis and application to the CROCUS experimental reactor. Ann. Nucl. Energy 101, 419–428.
Gerardin, D., Allibert, M., Heuer, D., Laureau, A., Merle, E., Seuvre, C., 2017. Design evolutions of Molten Salt Reactor. International Conference on Fast Reactors and Related Fuel Cycles: Next Generation Nuclear Systems for Sustainable Development (FR17). June 26-29.
Gidaspow, D., 1994. Multiphase Flow and Fluidization. Academic Press, New York.
Leppänen, J., Pusa, M., Viitanen, T., Valtavirta, V., Kaltiaisenaho, T., 2015. The Serpent Monte Carlo code: status, development and application in 2013. Ann. Nucl. Energy 82, 142–150.
Ranz, W.E., Marshall, W.R., 1952. Evaporation from droplets. Chem. Eng. Progress 48, 173–180.
Rusche, H., 2002. Computational Fluid Dynamics of Dispersed Two-Phase Flows at High Phase Fractions, PhD thesis.
Santamarina, A., Bernard, D., Blaise, P., Coste, M., Courcelle, A., Huynh, T.D., Jouanne, C., Leconte, P., Litaize, O., Ruggiéri, J-M., Sérot, O., Tommasi, J., Vaglio, C., Vidal, J-F., 2009. The JEFF-3.1.1 Nuclear Data Library, JEFF Report 22, OECD/NEA.
Serp, J., Allibert, M., Beneš, O., Delpech, S., Feynberg, O., Ghetta, V., Heuer, D., Holcomb, D., Ignatiev, V., Kloosterman, J.L., Luzzi, L., Merle, E., Uhlíř, J., Yoshioka, R., Zhimin, D., 2014. The molten salt reactor (MSR) in generation IV: overview and perspectives. Prog. Nucl. Energy 77, 308–319.
Stacey, W.M., 2007. Nuclear Reactor Physics. Wiley-VCH, Weinheim.
Tano, M., Rubiolo, P., Doche, O., 2017. Progress in modelling solidification in molten salt coolants. Model. Simul. Mater. Sci. Eng. 25, 1–29.
Tuominen, R., Valtavirta, V., Peltola, J., Leppänen, J., 2016. Coupling serpent and OpenFOAM for neutronics – CFD multi-physics calculations. PHYSOR 2016: Unifying Theory and Experiments in the 21st Century. May 1-5.